Resolving the Ultrafast Intersystem Crossing in a Bimetallic Platinum Complex

Andrew J. S. Valentine,¹ Joseph J. Radler,¹ Alexis Mills,¹ Pyosang Kim,² Felix N. Castellano,³ Lin X. Chen,² and Xiaosong Li^{1, a)}

(Dated: 16 August 2019)

Bimetallic platinum complexes have interesting luminescent properties and feature long-lasting vibrational coherence and ultrafast intersystem crossing after photoexcitation. Ultrafast triplet formation is driven by very strong spin-orbit coupling in these platinum (II) systems, where relativistic theoretical approaches beyond first-order perturbation theory are desirable. Using a fully variational relativistic theoretical method recently developed by the authors, we investigate the origins of ultrafast ISC in the $[Pt(ppy)(\mu^{-t}Bu_2pz)]_2$ complex (ppy=phenylpyridine, pz=pyrazolate). Spin-orbit coupling values, evaluated along a Born-Oppenheimer molecular dynamics trajectory, are used to propagate electronic populations in time. Using this technique, we estimate ultrafast intersystem crossing rates of 15-134 fs in this species for the possible intersystem crossing pathways into the three low-lying triplet states.

¹⁾Department of Chemistry, University of Washington, Seattle, WA, 98195

²⁾Chemical Sciences and Engineering Division, Argonne National Laboratory, Lemont, IL 60439, USA; Department of Chemistry, Northwestern University, Evanston, IL 60208, USA

³⁾Department of Chemistry, North Carolina State University, Raleigh, NC, 27695-8204

^{a)}Electronic mail: xsli@uw.edu

I. INTRODUCTION

Platinum (II) complexes have been well-studied due to their luminescent properties. As a result of their strong spin-orbit coupling, such complexes phosphoresce efficiently and are good candidates for organic light-emitting diodes (OLEDs).^{1,2} Platinum dimer complexes such as tetrakis(pyrophosphito)diplatinate(II) ($[Pt_2(pop)_4]^{4-}$), being smaller than large supramolecular systems and thus easier to control, nevertheless exhibit many of the same photophysical characteristics and have been extensively studied experimentally³⁻⁵ and theoretically.^{6,7} A series of binuclear platinum complexes with different bridging and cyclometalating ligands have been synthesized, forming a full library of bichromophoric metal complexes with subtly different electronic structure.⁸⁻¹⁰ This new generation of butterfly-shaped platinum dimers, such as the $[Pt(ppy)(\mu-^tBu_2pz)]_2$ complex (ppy=phenylpyridine, pz=pyrazolate) shown in Fig. 1, experimentally evinces rapid intersystem crossing (ISC) and long-lasting vibrational coherence after photoexcitation.¹¹⁻¹⁴

FIG. 1. Molecular structure for the ^tBu-substituted pyrazolate-cyclometalated diplatinum complex.

Recent theoretical work from the authors¹⁵ demonstrated that the long-lived (\sim 20 fs)

electronic coherence in the singlet metal-metal to ligand charge transfer (1 MMLCT) states of binuclear platinum complexes can be achieved through structural modifications of the bridging pyrazolate ligands that sterically enforce certain inter-platinum distances. However, pure electronic S_1 - S_2 coherence quickly collapses to the S_1 electronic state within 20 fs due to the coupling with molecular vibrations. The next stage of the ultrafast photochemical process in binuclear platinum complexes is the intersystem crossing to a triplet manifold, experimentally reported to take place before 150 fs after photoexcitation. In this paper, we continue to investigate the cascading excited-state pathway in photoexcited $[Pt(ppy)(\mu^{-t}Bu_2pz)]_2$ by studying the energetic landscape that supports the intersystem crossing dynamics from S_1 to lower-lying triplet states.

II. METHODOLOGY

A. Theory

Intersystem crossing, the transition between states of different spin multiplicities that is formally spin-forbidden within non-relativistic quantum mechanics, plays an important role in photochemistry. This change of spin state is only possible through spin-orbit coupling, a fundamentally relativistic phenomenon.^{17,18} We have recently developed a non-perturbative, variational approach based on relativistic theory to compute the spin-orbit coupling strength between spin-pure states.¹⁹ We only present a brief review herein and refer readers to Ref. 19 for theoretical details.

To observe a change in population between different spin states, a basis of states must first be selected, and then couplings between those states must be evaluated. As states calculated variationally in the presence of spin-orbit coupling will no longer belong to a pure spin state, but rather a superposition of several spin states, it is natural to perform calculations in a spin-pure basis where singlets, triplets, etc., can be easily identified. As such, we define spin-pure states to be our spin-diabatic basis, and spin-orbit-coupled states to be our spin-adiabats. In order to generate these, we apply a spin separation technique so

that the Dirac Hamiltonian can be written as,^{20,21}

$$\mathbf{H} = \begin{pmatrix} V & \hat{T} \\ \hat{T} & \frac{\mathbf{p}V \cdot \mathbf{p} - \hat{T}}{4m^2 c^2} \end{pmatrix} + \begin{pmatrix} \mathbf{0}_2 & \mathbf{0}_2 \\ \mathbf{0}_2 & \frac{i\boldsymbol{\sigma} \cdot \mathbf{p}V \times \mathbf{p}}{4m^2 c^2} \end{pmatrix}$$
(1)

where V is the scalar potential, \hat{T} the kinetic energy operator, c the speed of light, and m the electron mass. Spin and orbital angular momenta are coupled through the $\sigma \cdot \mathbf{p}V \times \mathbf{p}$ term: the vector σ contains the Pauli spin matrices, and \mathbf{p} is the linear momentum operator. The first term in Eq. (1) is the spin-pure portion of the Dirac Hamiltonian, which contains scalar relativistic effects, while the second term gives rise to spin-couplings.

Variationally solving the Dirac equation without the spin-orbit-coupling term will produce spin-diabatic states, e.g., singlets, triplets, etc., denoted as $\{\widetilde{\psi}_K\}$. In contrast, when spin-couplings are included in the Dirac Hamiltonian, the resulting eigenstates, $\{\psi_L\}$, correspond to spin-adiabatic states. In order to calculate the state-to-state couplings between states of different multiplicities, we search for a unitary transformation matrix, \mathbf{T} , relating $\{\psi_L\}$ and $\{\widetilde{\psi}_K\}$ (see Ref. 19 for details). Finally, taking the diagonal spin-adiabatic Hamiltonian \mathbf{H}

$$\mathbf{H} = \begin{bmatrix} E_1 & & & \\ & \ddots & & \\ & & E_M \end{bmatrix} \tag{2}$$

and rotating it into the spin-diabatic basis

$$\widetilde{\mathbf{H}} = \mathbf{T}\mathbf{H}\mathbf{T}^{\dagger} = \begin{bmatrix} \widetilde{E}_1 & V_{12} & \cdots \\ V_{12}^* & \widetilde{E}_2 \\ \vdots & & \ddots \end{bmatrix}$$

$$(3)$$

yields a diabatic Hamiltonian in a spin-pure basis with off-diagonal spin-orbit couplings that drive the intersystem crossing event. For the purpose of this work, nonadiabatic couplings between triplet states are effectively neglected, as we are principally interested in the transition from singlet to triplet. Once the spin-orbit couplings can be evaluated, what remains is to sample the nuclear configurations that result during the photoexcitation process; we elect to perform a single Born-Oppenheimer molecular dynamics (BOMD) trajectory on the

first singlet excited state, which will produce representative nuclear geometries for the early times of the photoexcited dynamics.

In this work, we employ the exact-two-component $(X2C)^{22-34}$ transformed relativistic time-dependent density-functional theory $(TDDFT)^{34-36}$ method to compute spin-diabatic and spin-adiabatic states, using the one-electron Dirac Hamiltonian without and with the spin-orbit coupling term. To account partially for two-electron relativistic effects, the spin-orbit operator within X2C is scaled by a semiempirical fudge factor,³⁷ reminiscent of the use of effective nuclear charges to account for nuclear screening of valence electrons by core electrons.

III. COMPUTATIONAL DETAILS

All calculations were performed using a locally modified copy of the development version of GAUSSIAN16.³⁸ Geometries for the platinum dimer were optimized³⁹ using the CAM-B3LYP functional,⁴⁰ the 6-31g(d) basis on light atoms, and the LanL2DZ effective core potential and double- ζ basis set on the Pt atoms.⁴¹ The range-separated functional was employed in order to better describe the excited states of this species, many of which are charge transfer in character;⁴² a comparison of different functionals is presented in the Supporting Information. Born-Oppenheimer molecular dynamics of the first singlet excited state were performed at the same level of theory, beginning at the ground state geometry with zero initial momentum, evaluated at 0.5 fs time steps over 200 fs. Relativistic X2C-TDDFT calculations were performed with the same functional and basis on light atoms, with the relativistic Sapporo double- ζ basis applied to Pt.⁴³ All non-relativistic density functional theory calculations were performed on a pruned (75, 302) grid (Grid=UltraFine in GAUSSIAN16), while the convergence of relativistic calculations was improved by switching to a pruned (175, 974) grid for light atoms and an unpruned (250, 974) grid for Pt (Grid=SuperFine).

IV. RESULTS AND DISCUSSION

Before discussing the dynamics, much information can be gleaned from static calculations at the ground- and excited-state geometries of the $[Pt(ppy)(\mu^{-t}Bu_2pz)]_2$ dimer complex, shown in Fig. 2 and given in full in the Supporting Information. Relative to the ground

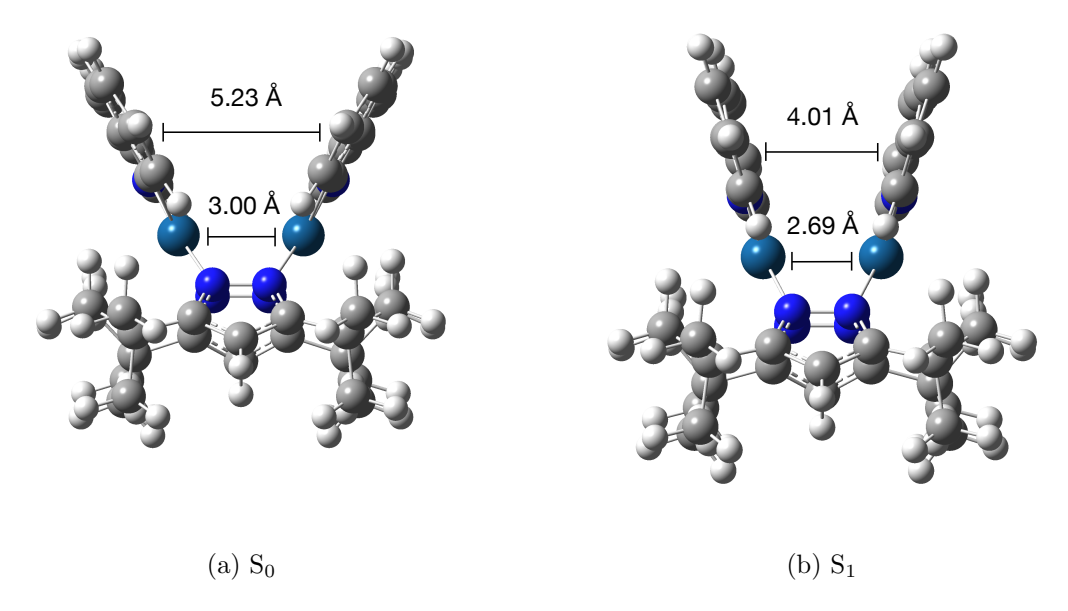


FIG. 2. Optimized geometries for the ground (a) and first singlet excited (b) states of the platinum dimer. The dimer contracts upon photoexcitation.

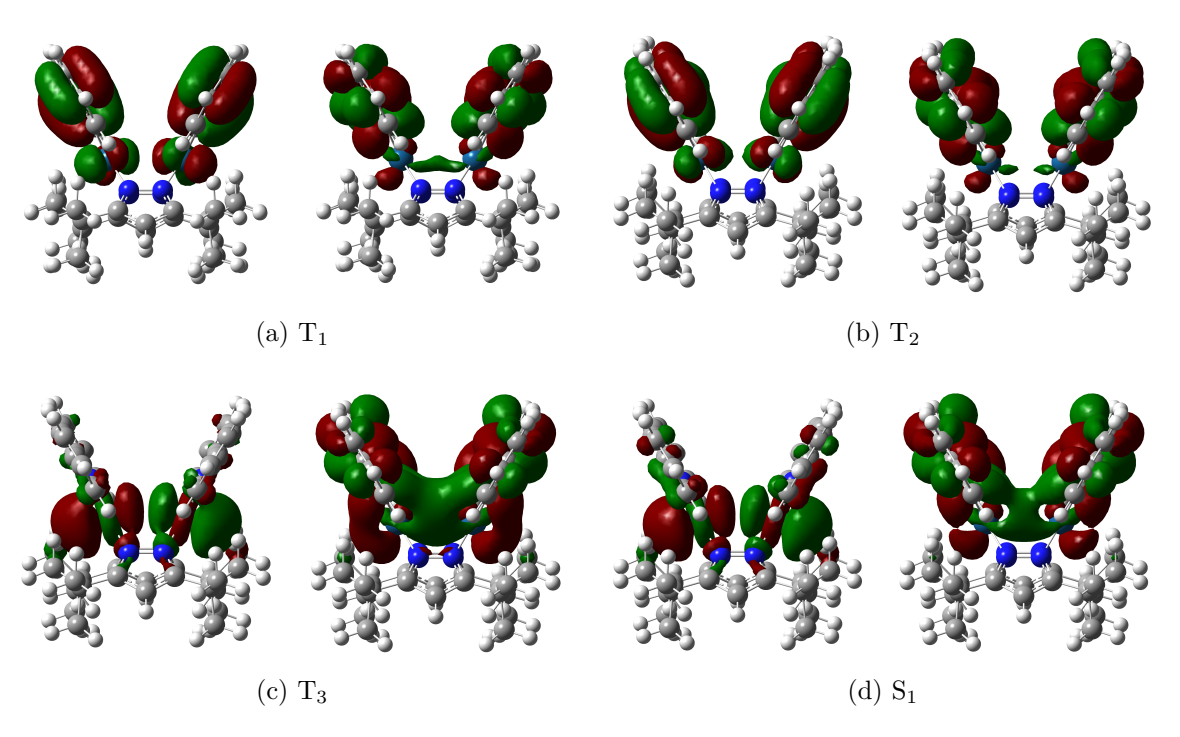


FIG. 3. (a)-(d): Natural transition orbitals (NTOs) of the first four excited states at the groundstate geometry, corresponding to a vertical excitation. For each state, the hole orbital is on the left and the particle orbital is on the right. T_1 and T_2 are LC, while T_3 and S_1 are MMLCT.

TABLE I. Spin-orbit coupling matrix elements V_{ST} of the four lowest-energy triplets to S_1 at the ground-state geometry, and the corresponding intersystem crossing rates Γ_{ST}^{-1} estimated from Fermi's Golden Rule. Intersystem crossing is fastest to T_2 , with non-negligible transition probabilities to the other triplets as well.

	T_1	T_2	T_3	T_4
$\overline{\mathrm{V}_{ST} \; (\mathrm{meV})}$				31
Γ_{ST}^{-1} (fs)	134	15	66	110

state, the Pt-Pt bond distance in S_1 contracts from 3.0 Å to 2.69 Å, and the phenylpyridine ligands fold toward one another, with their separation decreasing from 5.23 Å to 4.01 Å. This behavior can be explained by examining the natural transition orbitals (NTOs)⁴⁴ that correspond to an electronic transition from the ground state to the state of interest, plotted in Fig. 3. The S_1 state, which is a metal-metal-to-ligand charge-transfer (MMLCT) state, promotes an electron from the antibonding d_{z^2} orbital between the two Pt atoms to a bonding combination of π^* orbitals on the ppy ligands. This increases the bond order both between the Pt atoms and between the ppy ligands, resulting in shorter separations between each. At the ground-state geometry, there are three triplet states below S_1 in energy. T_1 and T_2 are ligand-centered (LC) states, while T_3 is also MMLCT. Though not shown, at the S_1 geometry, S_1 remains MMLCT and S_2 remains LC, while S_1 are the Supporting Information.

El-Sayed's rules⁴⁸ maintain that ISC is fastest between singlets and triplets that differ in electronic character. T_2 is the only triplet that is LC at both geometries, while S_1 is MMLCT. In addition, T_2 is lower in energy than S_1 at the ground-state geometry, while it is higher in energy at the S_1 minimum, implying there is a crossing between the two states somewhere between the two geometries. Those two facts allow us to postulate that T_2 is the most likely candidate for ultrafast ISC. However, using the procedure outlined above, it is possible to be more quantitative. The spin-orbit couplings at the ground-state geometry between the four lowest-energy triplets and S_1 are shown in Tab. I. As expected, the coupling to T_2 is quite strong at 84 meV (680 cm⁻¹), which is easily strong enough to allow for ultrafast intersystem crossing. A crude estimate for the ISC rate can be obtained

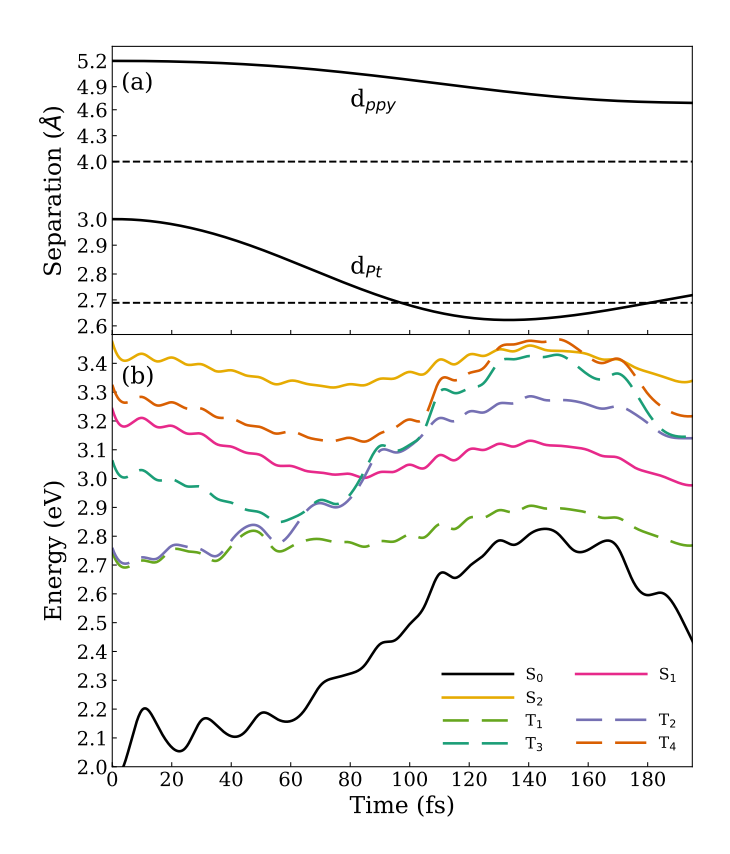


FIG. 4. Non-relativistic Born-Oppenheimer molecular dynamics simulation along the S_1 surface of the platinum dimer. (a) Geometric parameters as a function of time. The distance between the platinum atoms and between the ppy ligands both decrease over the early times of the simulation. Dashed lines indicate the value of these parameters at the S_1 equilibrium geometry. Note the different scales on the y-axis for the two parameters. (b) The potential energy surface (PES) of the low-lying singlet and triplet states relative to the ground-state energy at equilibrium (S_0 shifted 2.0 eV for clarity). S_1 reaches a relative minimum, and intersects with T_2 and T_3 , at 85 fs with a Pt-Pt bond distance of 2.72 Å.

by inserting these coupling values into Fermi's Golden Rule,

$$\Gamma_{if} = \frac{2\pi}{\hbar} |\langle f|\hat{H}|i\rangle|^2 \rho(E_f), \tag{4}$$

and neglecting the density-of-states by setting $\rho(E_f) = 1 \text{ eV}^{-1}$. Shown also in Tab. I, the ISC rate is fastest between the S₁ and T₂ states, at a rate of 15 fs. The ISC rates to the other triplets are slower, but are nevertheless still considered to be ultrafast events, with rates ranging from 66 fs to 134 fs—all faster than the experimental resolution of 150 fs.

While these static data are compelling evidence of ultrafast intersystem crossing to the second triplet excited state, ISC is an inherently dynamic process. ¹⁸ In order to qualitatively incorporate some of the photoexcited dynamics into the study of this molecule, an *ab initio*

direct Born-Oppenheimer molecular dynamics (BOMD)^{49,50} trajectory was performed for 200 fs on the S_1 surface, at the same TD-CAM-B3LYP/LanL2DZ level of theory as above. The simulation began from the Frank-Condon point with zero initial momentum. The full potential energy surface (PES) at this level of theory is shown in Fig. 4b. At this level of theory, S_1 proceeds directly to the vicinity of the S_1 minimum, reaching a local energy minimum around t = 85 fs. In these first 85 fs, the Pt-Pt bond length (shown in Fig. 4a) decreases rapidly, from 3.0 Å to 2.72 Å, near the S_1 minimum value of 2.69 Å. The energy rises somewhat as the Pt-Pt bond length decreases past its equilibrium value to a minimum of 2.63 Å, after which it begins to turn back toward equilibrium. The ppy ligands, whose orientation is the second major change between the ground- and excited-state geometries (also shown in Fig. 4a), are much slower to react, steadily approaching one another over the course of the simulation but remaining far from the equilibrium separation of 4.01 Å.

Interesting dynamics are also visible in the triplet states over this range of geometries. As expected, S_1 intersects with both T_2 and T_3 , around the same time as it reaches its local energy minimum. The change in electronic character of these states over the course of the simulation is evident. S_1 remains MMLCT over the entire trajectory, and T_2 remains LC. However, T_1 is LC at short times, becoming MMLCT by t=85 fs, while T_3 follows the inverse pattern. This behavior is manifested within the PES: T_1 and T_2 track one another closely for the first 50 fs, after which they diverge and T_2 and T_3 then rise in energy together. From these dynamics, it is clear that the photodynamics are strongly downhill for the first 80 fs, where we therefore consider the BOMD results to be representative of configurations likely sampled at short times after photoexcitation. After that point, particularly if ISC is fast enough that lower-lying triplet states might be meaningfully populated, it is less clear that the BOMD simulation remains physically meaningful, and consequently we restrict ourselves to considering the first 60 fs of the simulation.

With nuclear configurations now sampled, what remains is to evaluate the spin-orbit coupling between excited states at these geometries. To that end, single-point calculations were performed every 1 fs over the first 60 fs using X2C-TDDFT with and without spin-orbit coupling, with the resultant surfaces shown in Fig. 5. The PESs of spin-diabatic X2C results (Fig. 5a) look much the same as those from the effective core potential. However, even in the absence of spin-orbit coupling, the explicit inclusion of scalar relativistic effects leads to an even earlier singlet-triplet crossing, occurring around t = 40 fs. Each triplet

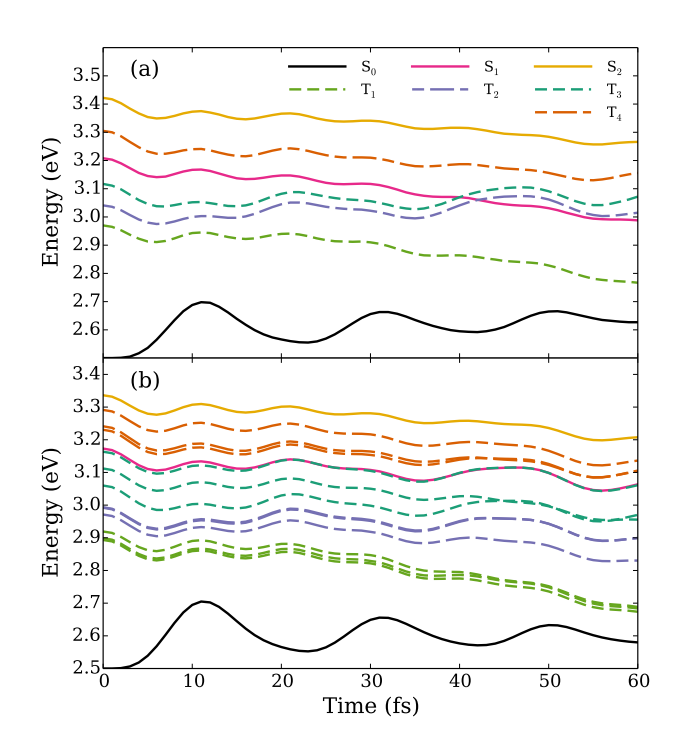


FIG. 5. Relativistic PES of the Pt dimer computed with X2C-TDDFT using geometries sampled from Born-Oppenheimer molecular dynamics simulations along the S_1 surface (S_0 shifted 2.5 eV for clarity). (a) Spin-diabatic PES predicts S_1 crossing the triplets T_2 and T_3 at an earlier time of 40 fs. (b) Spin-adiabatic PES shows that strong spin-orbit coupling dramatically changes the potential energy landscape, splitting triplets in energy by up to 0.1 eV and preventing the intersection of surfaces.

state in the spin-free X2C calculations correctly exhibits a three-fold degeneracy; for clarity, only one of each triplet state is shown in Fig. 5a. In contrast, a pronounced change occurs upon the inclusion of spin-orbit coupling (Fig. 5b). States that belong to the same triplet manifold are no longer degenerate and split in energy, by up to 0.1 eV in the case of T₃. The spin-orbit-coupled state corresponding to S₁ at short times is nearly flat over the trajectory, unlike its spin-diabatic counterpart, which steadily decreases in energy. While any degree of coupling between singlets and triplets would prevent true state crossings, one might expect to see several avoided crossings in regions where S₁ crossed triplet states in the spin-free calculations. Instead, there is very little change in relative energies along the trajectory, suggesting that spin-orbit coupling between states is strong relative to energetic differences. The dramatic change induced by spin-orbit coupling is evidence of very strong singlet-triplet interactions in the platinum dimer that lead to rapid ISC.

Using the procedure outlined above and detailed in Ref. 19, the spin-adiabatic states are rotated into the spin-diabatic basis, with the results plotted in Fig. 6a. Remarkably,

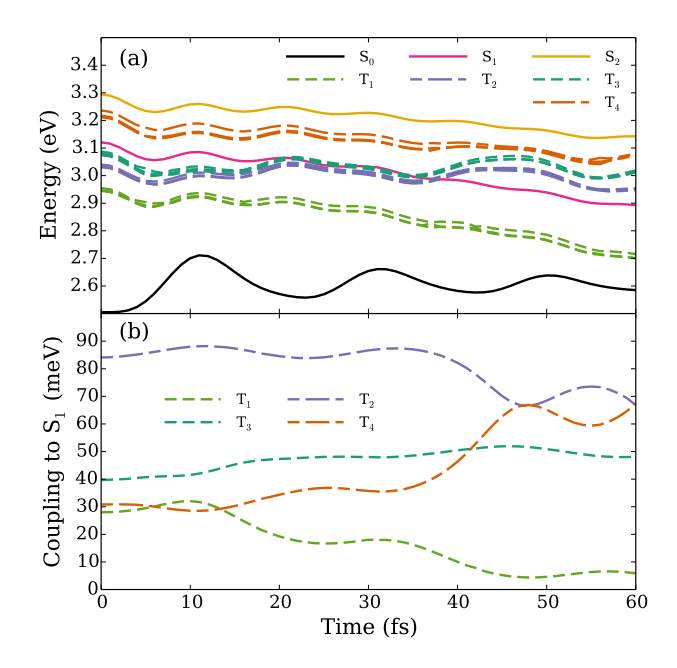


FIG. 6. (a) Energies of spin-adiabatic states rotated into the spin-diabatic basis. The diabatic transformation of the spin-adiabatic states recovers the qualitative character of the spin-diabatic states: the triplet states regain their degeneracies, and S_1 decreases in energy over time and crosses with T_2 and T_3 . (b) Diabatic coupling of triplet states to S_1 . The norm of each set of singlet-triplet couplings is presented. T_2 couples most strongly, by nearly 90 meV over the first 40 fs.

the qualitative character of the spin-pure results is almost completely recovered; S_1 again decreases in energy, triplets nearly regain their degeneracy, and there is a clear state crossing between S_1 and the triplets T_2 and T_3 . The diabatic couplings to S_1 from the various triplet states are also plotted in Fig. 6b. Singlet-triplet spin-orbit coupling is very strong in this species. As expected, T_2 couples most strongly to S_1 , by nearly 90 meV (725 cm⁻¹) over the first 40 fs. Coupling to T_3 and T_4 is also significant, varying from 30 meV to 65 meV, while the S_1 - T_1 coupling strength averages only 17 meV. However, this does not rule out the importance of the T_1 state in the photochemical process because it can couple to other triplet states after the ISC occurs.

Finally, the effect of spin-orbit coupling on singlet and triplet populations immediately following photoexcitation can be explored by directly propagating the populations according to

$$\boldsymbol{c}(t + \Delta t) = \exp\left[\frac{-i\widetilde{\boldsymbol{H}}\Delta t}{\hbar}\right]\boldsymbol{c}(t),\tag{5}$$

where $c_i(t)$ is the coefficient of state $\widetilde{\psi}_i$ at time t, and where non-adiabatic coupling has been neglected. The resulting populations, equal to $|c_i(t)|^2$, are shown in Fig. 7 for the

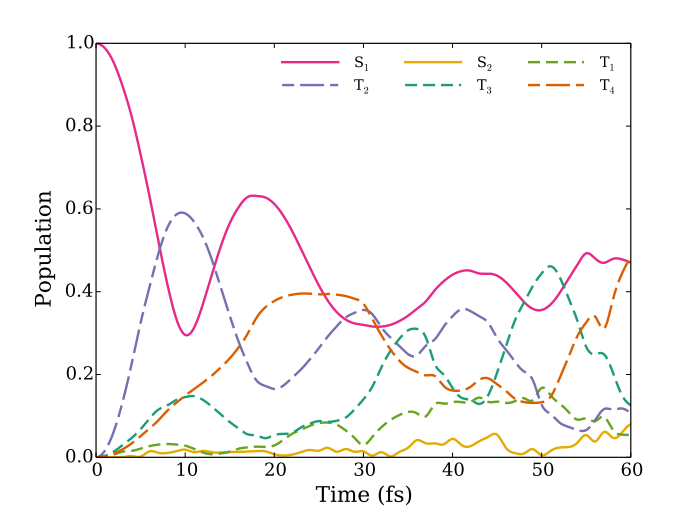


FIG. 7. Population dynamics driven by spin-orbit coupling over the first 60 fs. The S_1 population drops by 70% over the first 10 fs, followed by oscillatory behavior.

first 60 fs of the simulation, beginning with the total population in S_1 at time t = 0. A rapid depletion of S_1 is observed, dropping by 70% in just 10 fs. As expected, much of the population is transferred into T_2 , reaching an initial maximum of 60% at time t = 10 fs. After 10 fs, other triplets gain appreciable magnitude and oscillatory populations are observed. That the population of S_1 oscillates over time rather than steadily decreases is expected, as a consequence of a lack of coupling between triplet states. In particular, though the T_1 state is not efficiently populated in this simulation, it is lowest in energy and does not couple efficiently to S_1 ; were the triplet populations to funnel into T_1 , the reverse ISC reaction seen in the S_1 oscillations would be prevented. Transfer to T_1 can only be achieved through two factors neglected in this study: nonadiabatic coupling and vibronic effects. The former allows for direct population transfer between triplet states, while the latter can lead to broken symmetries and an increased internal conversion rate. Were these effects included, the intersystem crossing event would likely be rendered irreversible, and from these results, we predict the ISC rate to be under 15 fs.

V. CONCLUSION

In this work, we have demonstrated that strong spin-orbit coupling effects lead to ultrafast intersystem crossing in the $[Pt(ppy)(\mu^{-t}Bu_2pz)]_2$ dimer upon photoexcitation to the first singlet excited state. State-to-state spin-orbit couplings were evaluated using a variational

approach, applied to structures sampled from the *ab initio* excited-state molecular dynamics. The rate of ISC is evaluated using both Fermi's Golden Rule and time-propagation of state coefficients. Due to its LC electronic character, its low energy separation from S_1 , and its strong spin-orbit coupling to S_1 , the second triplet excited state T_2 is the most likely candidate for the initial ISC event. While the experimental resolution of intersystem crossing in this species is 150 fs, this work suggests the intersystem crossing event could occur within the first 15 fs, dramatically narrowing the window during which a change in spin state is likely to occur.

In the absence of explicitly evaluating nonadiabatic coupling between triplet states, and without allowing nuclear relaxation along triplet trajectories, nothing in the Hamiltonian in Eq. (3) will prevent the reverse ISC reaction. Development of analytical nuclear gradients, valuable in both nuclear dynamics and the evaluation of nonadiabatic coupling, remains therefore an important goal for variational relativistic methods. Future work will also consider the possibility of implicitly incorporating nonadiabatic coupling via a local diabatic transformation: 51,52 once triplet states can efficiently couple to T_1 , which does not meaningfully participate in the ISC, it is expected that the intersystem crossing will no longer appear reversible.

Finally, this work is evidence of the importance of choosing an appropriate basis for describing dynamical processes. Fully variational relativistic calculations, though more accurate in their depiction of spin-orbit coupling, render identification of the relevant states much more difficult, as it is no longer meaningful to speak of them as singlets or triplets. In contrast, after rotating into a spin-pure basis as above, states fully recover their multiplicities and are clearly identified. This procedure, in effect a form of spin-purification, is an important step in the use of variational relativistic calculations in the simulation of intersystem crossing events.

SUPPLEMENTARY MATERIAL

An analysis of excited-state character and density-functional dependence, as well as the ground- and excited-state geometries, are presented in the supplementary material.

ACKNOWLEDGMENTS

The development of two-component electronic structure method is funded by the US Department of Energy (DE-SC0006863). The development of non-perturbative spectroscopic methods is supported by the National Science Foundation (CHE-1856210). Computational intersystem crossing is partially supported by the U.S. Department of Energy, Office of Science, Office of Basic Energy Sciences, Division of Chemical Sciences, Geosciences and Biosciences, through Argonne National Laboratory under Contract No. DE-AC02-06CH11357. Computations were facilitated through the use of advanced computational, storage, and networking infrastructure provided by the Hyak supercomputer system at the University of Washington, funded by the Student Technology Fee and the National Science Foundation (MRI-1624430).

REFERENCES

- ¹J. G. Williams, S. Develay, D. L. Rochester, and L. Murphy, "Optimising the Luminescence of Platinum(II) Complexes and their Application in Organic Light Emitting Devices (OLEDs)," Coordin. Chem. Rev. **252**, 2596 2611 (2008).
- ²C.-L. Ho, W.-Y. Wong, B. Yao, Z. Xie, L. Wang, and Z. Lin, "Synthesis, Characterization, Photophysics and Electrophosphorescent Applications of Phosphorescent Platinum Cyclometalated Complexes with 9-arylcarbazole Moieties," J. Organomet. Chem. **694**, 2735–2749 (2009).
- ³R. M. van der Veen, C. J. Milne, A. El Nahhas, F. A. Lima, V.-T. Pham, J. Best, J. A. Weinstein, C. N. Borca, R. Abela, C. Bressler, and M. Chergui, "Structural Determination of a Photochemically Active Diplatinum Molecule by Time-Resolved EXAFS Spectroscopy," Angew. Chem. Int. Ed. 48, 2711–2714 (2009).
- ⁴R. M. van der Veen, A. Cannizzo, F. van Mourik, A. Vlček, and M. Chergui, "Vibrational Relaxation and Intersystem Crossing of Binuclear Metal Complexes in Solution," J. Am. Chem. Soc. **133**, 305–315 (2011).
- ⁵D. M. Roundhill, H. B. Gray, and C. M. Che, "Pyrophosphito-Bridged Diplatinum Chemistry," Acc. Chem. Res. **22**, 55–61 (1989).
- ⁶I. V. Novozhilova, A. V. Volkov, and P. Coppens, "Theoretical Analysis of the Triplet Excited State of the [Pt₂(H₂P₂O₅)₄]⁴⁻ Ion and Comparison with Time-Resolved X-ray and Spectroscopic Results," J. Am. Chem. Soc. **125**, 1079–1087 (2003).
- ⁷G. Levi, M. Pápai, N. E. Henriksen, A. O. Dohn, and K. B. Møller, "Solution Structure and Ultrafast Vibrational Relaxation of the PtPOP Complex Revealed by ΔSCF-QM/MM Direct Dynamics Simulations," J. Phys. Chem. C 122, 7100–7119 (2018).
- ⁸B. Ma, J. Li, P. I. Djurovich, M. Yousufuddin, R. Bau, , and M. E. Thompson, "Synthetic Control of Pt-Pt Separation and Photophysics of Binuclear Platinum Complexes," J. Am. Chem. Soc. **127**, 28–29 (2004).
- ⁹B. Ma, P. I. Djurovich, S. Garon, B. Alleyne, and M. E. Thompson, "Platinum Binuclear Complexes as Phosphorescent Dopants for Monochromatic and White Organic Light-Emitting Diodes," Adv. Func. Mater. **16**, 2438–2446 (2006).
- ¹⁰A. Chakraborty, J. E. Yarnell, R. D. Sommer, S. Roy, and F. N. Castellano, "Excited-State Processes of Cyclometalated Platinum(II) Charge-Transfer Dimers Bridged by Hy-

- droxypyridines," Inorg. Chem. **0**, 1298–1310 (2018).
- ¹¹J. V. Lockard, A. A. Rachford, G. Smolentsev, A. B. Stickrath, X. Wang, X. Zhang, K. Atenkoffer, G. Jennings, A. Soldatov, A. L. Rheingold, F. N. Castellano, and L. X. Chen, "Triplet Excited State Distortions in a Pyrazolate Bridged Platinum Dimer Measured by X-ray Transient Absorption Spectroscopy," J. Phys. Chem. A 114, 12780–12787 (2010).
- ¹²S. Cho, M. W. Mara, X. Wang, J. V. Lockard, A. A. Rachford, F. N. Castellano, and L. X. Chen, "Coherence in Metal–Metal-to-Ligand-Charge-Transfer Excited States of a Dimetallic Complex Investigated by Ultrafast Transient Absorption Anisotropy," J. Phys. Chem. A 115, 3990–3996 (2011).
- ¹³S. E. Brown-Xu, M. S. J. Kelley, K. A. Fransted, A. Chakraborty, G. C. Schatz, F. N. Castellano, and L. X. Chen, "Tunable Excited-State Properties and Dynamics as a Function of Pt-Pt Distance in Pyrazolate-Bridged Pt(II) Dimers," J. Phys. Chem. A 120, 543–550 (2016).
- ¹⁴P. Kim, M. S. Kelley, A. Chakraborty, N. L. Wong, R. P. Van Duyne, G. C. Schatz, F. N. Castellano, and L. X. Chen, "Coherent Vibrational Wavepacket Dynamics in Platinum(II) Dimers and Their Implications," J. Phys. Chem. C 122, 14195–14204 (2018).
- ¹⁵D. B. Lingerfelt, P. J. Lestrange, J. J. Radler, S. E. Brown-Xu, P. Kim, F. N. Castellano, L. X. Chen, and X. Li, "Can Excited State Electronic Coherence Be Tuned via Molecular Structural Modification? A First-Principles Quantum Electronic Dynamics Study of Pyrazolate-Bridged Pt(II) Dimers," J. Phys. Chem. A 121, 1932–1939 (2017).
- ¹⁶J. J. Radler, D. B. Lingerfelt, F. N. Castellano, L. X. Chen, and X. Li, "Role of Vibrational Dynamics on Excited-State Electronic Coherence in a Binuclear Platinum Complex," J. Phys. Chem. A 122, 5071–5077 (2018).
- ¹⁷C. M. Marian, "Spin-Orbit Coupling and Intersystem Crossing in Molecules," Wiley Interdiscp. Rev. Comput. Mol. Sci. 2, 187–203 (2012).
- ¹⁸T. J. Penfold, E. Gindensperger, C. Daniel, and C. M. Marian, "Spin-Vibronic Mechanism for Intersystem Crossing," Chem. Rev. 118, 6975–7025 (2018).
- ¹⁹A. Valentine and X. Li, "Toward the Evaluation of Intersystem Crossing Rates with Variational Relativistic Methods," J. Chem. Phys., accepted (2019).
- ²⁰K. G. Dyall and K. Fægri Jr., Introduction to Relativistic Quantum Chemistry (Oxford University Press, 2007).

- ²¹M. Reiher and A. Wolf, *Relativistic Quantum Chemistry*, 2nd ed. (Wiley-VCH, 2015).
- ²²W. Kutzelnigg and W. Liu, "Quasirelativistic Theory Equivalent to Fully Relativistic Theory," J. Chem. Phys. **123**, 241102 (2005).
- ²³W. Liu and D. Peng, "Infinite-Order Quasirelativistic Density Functional Method Based on the Exact Matrix Quasirelativistic Theory," J. Chem. Phys. **125**, 044102 (2006).
- ²⁴D. Peng, W. Liu, Y. Xiao, and L. Cheng, "Making Four- and Two-Component Relativistic Density Functional Methods Fully Equivalent Based on the Idea of 'From Atoms to Molecule'," J. Chem. Phys. 127, 104106 (2007).
- ²⁵M. Ilias and T. Saue, "An Infinite-Order Relativistic Hamiltonian by a Simple One-Step Transformation," J. Chem. Phys. 126, 064102 (2007).
- ²⁶W. Liu and D. Peng, "Exact Two-Component Hamiltonians Revisited," J. Chem. Phys. 131, 031104 (2009).
- ²⁷W. Liu, "Ideas of Relativistic Quantum Chemistry," Mol. Phys. **108**, 1679–1706 (2010).
- ²⁸T. Saue, "Relativistic Hamiltonians for Chemistry: A Primer," ChemPhysChem **12**, 3077–3094 (2011).
- ²⁹Z. Li, Y. Xiao, and W. Liu, "On the Spin Separation of Algebraic Two-Component Relativistic Hamiltonians," J. Chem. Phys. **137**, 154114 (2012).
- ³⁰D. Peng, N. Middendorf, F. Weigend, and M. Reiher, "An Efficient Implementation of Two-Component Relativistic Exact-Decoupling Methods for Large Molecules," J. Chem. Phys. 138, 184105 (2013).
- ³¹F. Egidi, J. J. Goings, M. J. Frisch, and X. Li, "Direct atomic-orbital-based relativistic two-component linear response method for calculating excited-state fine structures," J. Chem. Theory Comput. 12, 3711–3718 (2016).
- ³²J. J. Goings, J. M. Kasper, F. Egidi, S. Sun, and X. Li, "Real time propagation of the exact two component time-dependent density functional theory," J. Chem. Phys. 145, 104107 (2016).
- ³³L. Konecny, M. Kadek, S. Komorovsky, O. L. Malkina, K. Ruud, and M. Repisky, "Acceleration of Relativistic Electron Dynamics by Means of X2C Transformation: Application to the Calculation of Nonlinear Optical Properties," J. Chem. Theory Comput. 12, 5823–5833 (2016).
- ³⁴F. Egidi, S. Sun, J. J. Goings, G. Scalmani, M. J. Frisch, and X. Li, "Two-Component Non-Collinear Time-Dependent Spin Density Functional Theory for Excited State Calcu-

- lations," J. Chem. Theory Comput. 13, 2591–2603 (2017).
- ³⁵J. M. Kasper, P. J. Lestrange, T. F. Stetina, and X. Li, "Modeling L_{2,3}-Edge X-ray Absorption Spectroscopy with Real-Time Exact Two-Component Relativistic Time-Dependent Density Functional Theory," J. Chem. Theory Comput. 14, 1998–2006 (2018).
- ³⁶A. Petrone, D. B. Williams-Young, S. Sun, T. F. Stetina, and X. Li, "An Efficient Implementation of Two-Component Relativistic Density Functional Theory with Torque-Free Auxiliary Variables," Euro. Phys. J. B 91, 169 (2018).
- ³⁷J. C. Boettger, "Approximate Two-Electron Spin-Orbit Coupling Term for Density-Functional-Theory DFT Calculations Using the Douglas-Kroll-Hess Transformation," Phys. Rev. B **62**, 7809–7815 (2000).
- ³⁸M. J. Frisch, G. W. Trucks, H. B. Schlegel, G. E. Scuseria, M. A. Robb, J. R. Cheeseman, G. Scalmani, V. Barone, G. A. Petersson, H. Nakatsuji, X. Li, M. Caricato, A. V. Marenich, J. Bloino, B. G. Janesko, R. Gomperts, B. Mennucci, H. P. Hratchian, J. V. Ortiz, A. F. Izmaylov, J. L. Sonnenberg, D. Williams-Young, F. Ding, F. Lipparini, F. Egidi, J. Goings, B. Peng, A. Petrone, T. Henderson, D. Ranasinghe, V. G. Zakrzewski, J. Gao, N. Rega, G. Zheng, W. Liang, M. Hada, M. Ehara, K. Toyota, R. Fukuda, J. Hasegawa, M. Ishida, T. Nakajima, Y. Honda, O. Kitao, H. Nakai, T. Vreven, K. Throssell, J. A. Montgomery, Jr., J. E. Peralta, F. Ogliaro, M. J. Bearpark, J. J. Heyd, E. N. Brothers, K. N. Kudin, V. N. Staroverov, T. A. Keith, R. Kobayashi, J. Normand, K. Raghavachari, A. P. Rendell, J. C. Burant, S. S. Iyengar, J. Tomasi, M. Cossi, J. M. Millam, M. Klene, C. Adamo, R. Cammi, J. W. Ochterski, R. L. Martin, K. Morokuma, O. Farkas, J. B. Foresman, and D. J. Fox, "Gaussian 16 Revision B.01," (2016), Gaussian Inc. Wallingford CT.
- ³⁹X. Li and M. J. Frisch, "Energy-Represented Direct Inversion in the Iterative Subspace within a Hybrid Geometry Optimization Method," J. Chem. Theory Comput. 2, 835–839 (2006).
- ⁴⁰T. Yanai, D. P. Tew, and N. C. Handy, "A New Hybrid Exchange–Correlation Functional using the Coulomb-attenuating Method (CAM-B3LYP)," Chem. Phys. Lett. **393**, 51–57 (2004).
- ⁴¹P. J. Hay and W. R. Wadt, "Ab Initio Effective Core Potentials for Molecular Calculations. Potentials for Potassium to Gold Including the Outermost Core Orbitals," J. Chem. Phys. **82**, 299–310 (1985).

- ⁴²A. J. Atkins and L. González, "Trajectory Surface-Hopping Dynamics Including Intersystem Crossing in [Ru(bpy)₃]²⁺," J. Phys. Chem. Lett. **8**, 3840–3845 (2017).
- ⁴³T. Noro, M. Sekiya, and T. Koga, "Segmented Contracted Basis Sets for Atoms H through Xe: Sapporo-(DK)-nZP Sets (n = D, T, Q)," Theor. Chem. Acc. **131**, 1124 (2012).
- ⁴⁴R. L. Martin, "Natural Transition Orbitals," J. Chem. Phys. **118**, 4775–4777 (2003).
- ⁴⁵A. V. Luzanov and O. A. Zhikol, "Electron Invariants and Excited State Structural Analysis for Electronic Transitions within CIS, RPA, and TDDFT Models," Int. J. Quant. Chem. **110**, 902–924 (2010).
- ⁴⁶F. Plasser and H. Lischka, "Analysis of Excitonic and Charge Transfer Interactions from Quantum Chemical Calculations," J. Chem. Theory Comput. 8, 2777–2789 (2012).
- ⁴⁷F. Plasser, M. Wormit, and A. Dreuw, "New Tools for the Systematic Analysis and Visualization of Electronic Excitations. I. Formalism," J. Chem. Phys. **141**, 024106 (2014).
- ⁴⁸M. A. El-Sayed, "Spin-Orbit Coupling and the Radiationless Processes in Nitrogen Heterocyclics," J. Chem. Phys. **38**, 2834–2838 (1963).
- ⁴⁹X. Li, J. M. Millam, and H. B. Schlegel, "Ab Initio Molecular Dynamics Studies of the Photodissociation of Formaldehyde, H₂CO→H₂ + CO: Direct Classical Trajectory Calculations by MP2 and Density Functional Theory," J. Chem. Phys. **113**, 10062–10067 (2000).
- 50 X. Li, J. M. Millam, and H. B. Schlegel, "Glyoxal Photodissociation. An Ab Initio Direct Classical Trajectory Study of $C_2H_2O_2 \rightarrow H_2 + 2CO$," J. Chem. Phys. **114**, 8897–8904 (2001).
- ⁵¹G. Granucci, M. Persico, and A. Toniolo, "Direct Semiclassical Simulation of Photochemical Processes with Semiempirical Wave Functions," J. Chem. Phys. 114, 10608–10615 (2001).
- ⁵²F. Plasser, G. Granucci, J. Pittner, M. Barbatti, M. Persico, and H. Lischka, "Surface Hopping Dynamics using a Locally Diabatic Formalism: Charge Transfer in the Ethylene Dimer Cation and Excited State Dynamics in the 2-pyridone Dimer," J. Chem. Phys. 137, 22A514 (2012).